IEEE Access
Multidisciplinary | Rapid Review | Open Access Journal

Received September 7, 2020, accepted October 10, 2020, date of publication November 9, 2020,
date of current version November 18, 2020.

Digital Object Identifier 10.1109/ACCESS.2020.3034593

Test and Comprehensive Evaluation for the Performance of UAV-Based Fertilizer Spreaders

CANCAN SONG, YING ZANG, ZHIYAN ZHOU, XIWEN LUO, LINGLI ZHAO, RUI MING, LE ZI, AND YU ZANG

College of Engineering, South China Agricultural University, Guangzhou 510642, China
Guangdong Engineering Research Center for Agricultural Aviation Application (ERCAAA), Guangzhou 510642, China
National Center for International Collaboration Research on Precision Agricultural Aviation Pesticides Spraying Technology (NPAAC), Guangzhou 510642, China
Key Laboratory of Key Technology on Agricultural Machine and Equipment (South China Agricultural University), Ministry of Education, Guangzhou 510642, China

Corresponding authors: Zhiyan Zhou (zyzhou@scau.edu.cn) and Ying Zang (yingzang@scau.edu.cn)

This work was supported in part by the National Key Research and Development Program of China under Grant 2018YFD0200301, in part by the National Natural Science Foundation of China under Grant 31871520, in part by the Project of Rural Revitalization Strategy in Guangdong Province under Grant 2020KJ261, in part by the Innovative Research Team of Agricultural and Rural Big Data in Guangdong Province of China under Grant 2019KJ138, and in part by the Project of Jiangsu Natural Science Youth Fund under Grant BK20160510.

ABSTRACT The feasibility of aerial fertilization by UAV-based granular fertilizer spreaders (GFSs) has been widely accepted. Although commercial UAV-based spreaders have emerged, their performance in granular fertilizer spreading application has rarely been studied. This paper tested the performances of four existing UAV-based GFSs in the automatic controllability, range of the discharge rate and the swath width and uniformity of the distribution. An analytic hierarchy process (AHP)-based method was proposed to evaluate their comprehensive performance in spreading application. The main results are as follows: (a) GFS-A showed the maximum controllable discharge rate of 27 kg/min, and GFS-B showed the minimum (proximately 3 kg/min). The discharge rate could be changed in a stepless way by GFS-B, C and D. The relationship between the discharge rate and the rotational speed of the fluted roller of GFS-D showed a significant linear relationship ($R^2 = 0.9991$) for the operational range. (b) The distribution patterns of GFS-A and D were trapezoidal, which was the better deposition pattern for generating uniform spreading; those of the other two UAV-based GFSs were a wide triangle with obviously asymmetrical sides (GFS-B) and a typical M-shape with two peaks (GFS-C). (c) the simulation of CV-swath width illustrated that the available effective swath width ($CV \leq 20\%$) for these UAV-GFSs were 5.1m ($CV = 14.73\%$), 4.8m($CV = 17.55\%$), 3.9m($CV = 13.02\%$) and 5.7m($CV = 18.36\%$) respectively under the given conditions. Furthermore, according to the AHP-based evaluation model, it was proved that GFS-D was able to provide superior performance in precise fertilization for a large application range, which is important for its practical application. This comparative study makes useful contribution for farmers and researchers in this field in understanding the application performance of various UAV-based GFSs.

INDEX TERMS Precision agriculture, unmanned aerial spreader, variable-rate fertilizer application, AHP, distribution pattern.

I. INTRODUCTION

As the main provider of nitrogen nutrients for high-yield crop production, granular fertilizer makes up a large part of agricultural chemical inputs [1]. Traditionally, mechanical fertilization was mainly performed using machines on the ground. Although their work efficiency and profit margins have been significantly improved, it is difficult for these machines to move in deep paddy fields and/or pass through crops where stem leaves are high enough to cover the row

The associate editor coordinating the review of this manuscript and approving it for publication was Shafiqul Islam.

This work is licensed under a Creative Commons Attribution-NonCommercial-NoDerivatives 4.0 License.
For more information, see https://creativecommons.org/licenses/by-nc-nd/4.0/

spacing [2], [3]. In addition, the unacceptable soil and land damage caused by the long-term field application of high-horsepower ground machines should not be ignored [4].

As a new agricultural machinery, agricultural UAV can be performed without touching the cultivated land surface and/or the crop canopy, offering an effective and flexible solution for special fields given the low adaptability and trafficability of ground machines [5]. Notably, manned fixed-wing aircrafts are applicable to large areas of connected agricultural fields [6], while UAVs are more suitable in irregular small-scale fields and hilly lands especially in Asia due to their flight flexibility and controllability [7]. Additionally, the performance improvements of agricultural UAVs especial in payload and flying capacity have recently increased rapidly, expanding its application in granule spreading [8], [9]. Furthermore, the development of precision technologies promotes the field application of agricultural UAVs with good distribution performance [10], [11].

The existing UAV-based spreaders are mainly divided into two types: the centrifugal disc type and the pneumatic type. Li *et al.* designed a centrifugal disc-type spreader mounted on a 12-axis UAV and verified its feasibility in a field experiment [12]. As an improvement, a seed fluted roller designed by Song *et al.* was mounted above the disc to generate a continuous particle flow falling on the disc. The position of the particle flow falling on the disc greatly influenced the distribution uniformity [4]. To generate a nonhollow deposition distribution in the field experiment, Wu *et al.* designed a baffle ring mounted around the disc for particle rebound. A bench test and a dynamic test of rice seeding were conducted before the field experiment [13]. The results of the field experiment using the optimum parameter settings evaluated in advance showed the feasibility of aerial spreading. Cointault, F. *et al.* designed an imaging technology to test and analyze the motion characteristic of fertilizer particle from a centrifugal spreader for a good application [14]. Although their working principle is simple, disc-type spreaders inherently result in variable swath deposition [15]. On the other hand, Song *et al.* designed an air-assisted spreader based on agricultural UAV. The particle motion affected by the interaction of the airflow from the duct and the wind field of the UAV was analyzed and optimized to obtain a better trajectory distribution [16]. Furthermore, a drill seeder was also designed and mounted on the UAV, which could force the particle flow to fall in rows. At the bottom of the drill seeder, the particle flow was carried by the airflow along a duct to the end with a sufficient final velocity. To date, several commercial UAV-based spreaders have emerged for agricultural material spreading applications and have attracted considerable attention.

Considering the differences in the working principle among the various UAV-based spreaders and the deviations between the desired and actual distributions in terms of the physical characteristics of the granular material [17], a performance evaluation is needed to provide a comprehensive understanding of the effects of parameter settings on discharge performance and deposition distribution. In order to improve accuracy of variable-rate technology in fertilization application, Fulton, J.P. *et al.* developed a spatial data model to evaluate the performance of two ground spreaders [18]. A specialized mathematical model and analysis tool were proposed by Grift to study the distribution patterns and factors influencing the deposition distribution [19]. In order to analyze the usage limitation of sowing by agricultural UAV in complex field, Wang, *et al.* developed a virtual simulation system for simulating agricultural material sowing. This portable and interactive system, equipped with 3D virtual scene construction, would give the user a perfect experience [20]. This analysis tool theoretically investigates the overall quality of spreading pattern shapes, which are associated with the swath width and uniformity. The overall results can be applied in field application and have a great influence on achieving effective spreading while minimizing application error. The objective of fertilization using UAV-based GFS is to spread fertilizer at a preset rate and an acceptable uniformity while minimizing the total flight route and operation time. Hence, an application performance evaluation is necessary to provide a detailed understanding of UAV-based GFS before their field application.

However, the relevant performance parameters of the existing commercially produced UAV-based spreaders have not been analyzed in terms of fertilizer discharge properties and spreading patterns. The goals of this study were to (a) compare the spreading performance and distribution patterns of four existing UAV-based GFSs to provide valuable technical reference and guidance for proper field application, and (b) explore the proper spreading method for achieving automatic variable-rate control of fertilizer application rate. Furthermore, these results could be an important basis for the further development of variable-rate fertilization using UAV-based GFS.

II. MATERIALS AND METHODS

A. UAV-BASED GRANULAR FERTILIZER SPREADERS

1) GRANULAR FERTILIZER SPREADERS

The four representative UAV-based GFSs used in the test (Fig. 5) are referred to as GFS-A, GFS-B, GFS-C and GFS-D. GFS-A and GFS-B are disc-type spreaders, which depend on a disc with paddles at the bottom of the hopper to disperse the particles falling from the hopper. The diameter and rotation speed of the disc are the main factors influencing the deposition distribution. GFS-A was mounted on a four-rotor UAV with a pair of propellers on each of rotor, while GFS-B was mounted on an eight-rotor UAV. GFS-C is a pneumatic-type spreader featuring a Y-shaped divider that forces the fertilizer flow to fall from the open valve into two main tube branches. The head of each tube branch is also divided into several outlets with the goal of increasing the dispersion width and spreading uniformity in terms of the structural design. GFS-D is a pneumatic-type spreader equipped with a pneumatic conveying system. Inside of the pneumatic conveying system, the divider could divide the

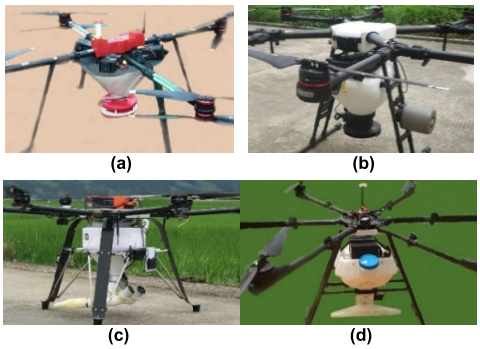

FIGURE 1. Four types of the UAV-GFSs used in the test. (a) GFS-A (b) GFS-B (c) GFS-C (d) GFS-D.

airflow from the fan into all ducts, and then the gas-solid two-phase flow moved through the pneumatic ducts at a high speed, ensuring a simple and controllable trajectory in the air. Table 1 shows the main characteristics of these four UAV-based GFSs.

TABLE 1. Specification of test UAV-based GFS.

Property	GFS-A	GFS-B	GFS-C	GFS-D
Propeller number	8	8	6	6
Maximum load (kg)	20	8	16	20
Height (m)	4-7	4-7	4-7	4-7
Speed(m/s)	5-7	5-7	5-7	5-7
Power resource	lithium battery 52V	lithium battery 44.4V	lithium battery 50.4V	lithium battery 50.4V
Spreader type	centrifugal disc	centrifugal disc	pneumatic double-duct	pneumatic multi-duct
Particle diameter(mm)	0.5-5	0.5-5	0.5-5	0.5-5

2) FERTILIZER DISCHARGE APPARATUS

The discharge mechanisms of the UAV-GFSs follow the different principles, as do their metering devices. As is shown in Fig.2(a), the plastic annulus mounted on the bottom of GFS-A is used to adjust the discharge rate by manually replacing the annulus with different diameter. Fig.2(b) shows metering device in GFS-B. A flabellate outlet gate is mounted at the bottom of material hopper, and a straight board, moving forward and back in the horizontal plane, is set under the flabellate gate for achieving variable discharge rates. A butterfly valve shown in the Fig.2(c) is set at the bottom of the material hopper mounted on the GFS-C. Consisted of two semicircular blades, the butterfly valve rotates around the central axis at the desired angle for outlets of different sizes. As shown in Fig.2(d), the fertilizer discharge apparatus of GFS-D is a fluted roller, optimized in effective work length, flute diameter and number of flutes to meet the requirement of fertilizer discharge rate [21]. The rotational fluted roller forces the particle out at different rotational speeds, achieving stepless variable-rate application.

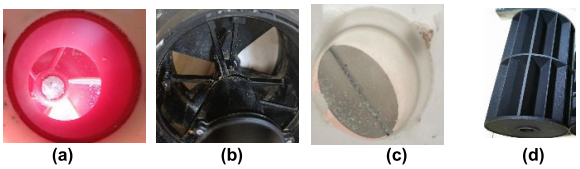

FIGURE 2. Schematic diagram of discharge constructions of the UAV-GFSs. (a) Annulus for GFS-A. (b) Straight board for GFS-B. (c) Butterfly valve for GFS-C. (d) Fluted roller for GFS-D.

The discharge properties of these four kinds of discharge structures are listed in table 2.

TABLE 2. Specifications of the idscharge structures.

Property	GFS-A	GFS-B	GFS-C	GFS-D
Discharge construction	annulus outlet	sector outlet	butterfly valve	fluted roller
Variate	diameter	outlet opening ratio	angle	rotational speed
Variable range	20 mm-37 mm	0-100 percent	0-90 degree	0-100 rpm
Stepless adjustment	no	yes	yes	yes

B. PHYSICAL PROPERTIES OF GRANULAR FERTILIZER

The fertilizer used in this study was granular urea, and its nitrogen content was more than 46.4%. The diameter of the urea particles was 1.18-3.35 mm, the bulk density was 0.72 g/ml, and one thousand particles weighed 4.65 g.

C. TEST OF FERTILIZER DISCHARGE APPARATUSES

A set of experiments on discharge performance was carried out under static laboratory condition, eliminating the influence of the external vibrations caused by the UAVs. The amount of urea in the hopper (8 kg) remained unchanged in all tests, and the time required to discharge all the urea was measured. These measurements were used to calculate the mass flow rate (in kg/min). Available parameter settings were taken to change the gate openings of the discharge structures. The tested variable values for various gate openings were as follows: the annulus diameters of GFS-A were 20 mm, 28 mm, 30 mm, 33 mm and 37 mm; the opening ratio of GFS-B was from 40% to 100% with an interval of 10%; the opening angle of GFS-C was from 45° to 75° with an interval of 5°; and the rotation speed of GFS-D was 5-60 r/min with an interval of 10 r/min starting at the speed of 10 r/min. All measurements occurred with three replicates.

D. TEST OF DEPOSITION DISTRIBUTION

The dynamic test was carried out in wind tunnel experiment base of South China Agricultural University located in Guangzhou city, China. The meteorological condition of field temperature was 26°C-35°C, northwest wind speed was 1.61m/s-2.03m/s and relative humidity was about 65%. All tests were run at constant altitude and urea weight in the hopper. The within-swath deposition of UAV-based GFSs over

a range of material application rates commonly associated with precision agriculture schemes was analyzed.

1) TEST CONDITION

Table 3 shows the work parameters and test conditions for all four UAV-based GFSs for the distribution pattern experiment. To acquire a valid deposition result along collection lines, the moderate discharge rates and travel speed of the UAV-based GFSs were adjusted. Namely, the flight speed of GFS-A was set at 1.5m/s to prevent urea particle from being blow away by the strong wind field generated by coupled propellers. Considering the small discharge rate of GFS-B, the flight speed of was set at 1.2m/s with the goal of obtaining effective deposition amount in sampling area. The flight speed of the rest of UAV-based GFSs was 2.0 m/s. The rotational speeds of the discs for GFS-A and B and the air velocity of the air-assisted tubes for GFS-C and GFS-D were set appropriately according to the results of preliminary experiment.

TABLE 3. Test parameters and conditions.

Property	GFS-A	GFS-B	GFS-C	GFS-D
Urea (kg)	8	8	8	8
Altitude (m)	3	3	3	3
Flight speed (m/s)	1.5	1.2	2.0	2.0
Outlet size	20 mm	70%	50°	30 r/min
Discharge rate (kg/min)	4.95	2.94	4.52	5.4
Disc speed (r/min)	700	700	-	-
Tube branch angle (°)	-	-	68	130
Air velocity in the tube (m/s)	-	-	20	8.2

2) SAMPLING METHOD

A large rectangular collection carpet was placed on the ground for urea sample collection. The soft carpet was long enough to prevent the particles from bouncing around. The carpet was divided into 39 collection points with several fixed straight lines. Every collection point was divided into three small square grids (0.3×0.3 m) parallel to the forward direction, forming three sample lines perpendicular to the overall forward direction. The collection carpet was oriented so that the UAV-based GFS will be flying directly into the wind to minimize the effects of crosswind in the distribution pattern. A colored belt used to guide the proposed flight line was set along the collection carpet centerline. A remote controller with a screen recorded the flight deviation, travel speed and altitude of each flight by using ground station equipment. After taking photographs of the urea samples on the collection carpet in individually identified grids, the images were uploaded into a computer system to determine the number of particles in each grid with MATLAB software (version 2016). In the case of the urea particle, the quantity was converted to grams per square meter using the weight of one thousand particles. The deposition distribution of all grids was plotted in a bar graph. The mean values (g/m^2) of the three grids at one collection point versus the collection points were plotted in the form of distribution curves. Three repetitions were performed in every test. Fig. 3 shows the collection conditions for the distribution patterns. All tests were performed according to the method described in ASAE Standard [22].

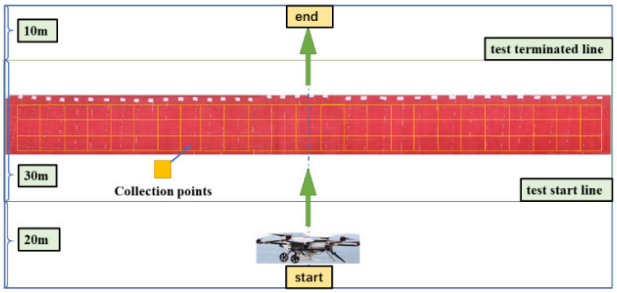

FIGURE 3. Distribution of collection points in the test field.

E. EVALUATION INDICES

The evaluation indices were not only used for recommendation in field application, but also as the reference for selecting a suitable UAV-based GFS for the development of a variable-rate fertilization control system.

When applying UAV-based GFSs, the controllable range and the variable-rate control mode are the basic performance references for selecting a certain discharge apparatus to improve work efficiency. A larger controllable range makes it easier to meet the requirements of discharging a large quantity of granular fertilizer. It is noteworthy that the accurate and stepless control mode of the discharge apparatus have great significance in variable-rate application by UAV-based GFS [23]. The relationship between the values of openings of metering devices and the discharge rates will be studied for automatic adjusting.

To visually illustrate the deposition distribution patterns, the collected urea samples were analyzed in terms of the particle quantities in different collecting lines and the deposition area along the direction perpendicular to the forward direction. The overall trend in the deposition distribution represents the actual spreading performance of UAV-based GFS, and a better deposition pattern for spreading is determined based on the space between routes where overlaps and misseeding easily occur. It is widely accepted that a good distribution pattern should be symmetric with the target discharge rate near the centerline and should decrease monotonically at both ends of the collection line.

The effective swath width and the uniformity of distribution were the two main indices for evaluating the spreading performance of UAV-based GFS [24]. These indices directly influence the work efficiency and spreading quality of UAV-based GFS. The coefficient of variation (CV) was used to illustrate the uniformity of the deposition distribution. The method is to analyze the relationship of the CV to the

swath width by overlapping the swaths of the single-pass distribution pattern in the same direction [22]. The CV of the deposition distribution from the centerline of the first swath to the centerline of the third swath is calculated by using equations (1)-(3). In general, the simulated curve should reach a minimum, and the best swath width is associated with the minimum CV (Fig.4); in practice, the maximum swath width with a related CV under the given standard line (usually decided by the field application) is widely acceptable.

$$\overline{M} = \frac{\sum M_i}{n} \tag{1}$$

$$\mathrm{SD} = \frac{\sqrt{\sum_1^n (M_i - \overline{M})^2}}{n-1} \tag{2}$$

$$\mathrm{CV} = \frac{SD}{\overline{M}} \tag{3}$$

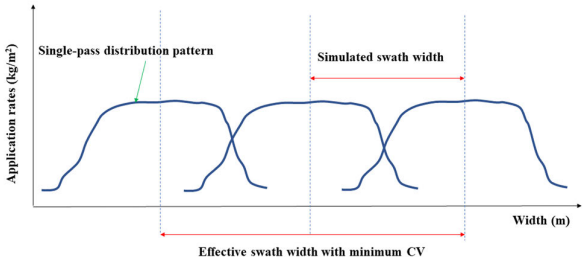

FIGURE 4. Graphical presentation of deposition pattern in simulated method.

where n = the number of collection points, n = 39; M_i = the mean of three deposition quantities at a collection point (g); $\overline{M}$ = the mean of all collection points (g); and SD = the standard error (g).

F. COMPREHENSIVE EVALUATION MODEL

As it was difficult to make a quantitative decision with these evaluation indices, an analytic hierarchy process (AHP)–based method [25] was proposed to rank the prioritized options for implementing a variable-rate fertilization control system with the UAV-based GFS.

The AHP method consisted of three basic steps: first, the problem was broken down and structured into a hierarchy of subproblems, and a hierarchical model was built; second, the data were collected and measured through pairwise comparisons of the attributes, and a comparison matrix was constructed; finally, the priority weights of the factors in each level were calculated, and a consistency check was performed [26].

A hierarchy model includes a target layer, a criterion layer and a scheme layer. In this study, the target layer was exploring the importance of the evaluation indices. The criterion layer consisted of automatic controllability, the range of the discharge rate, the swath width and the uniformity of the distribution. The scheme layer included the four types of UAV-based GFSs. The hierarchy model for all categories and indices was classified into three levels, as shown in Fig. 5.

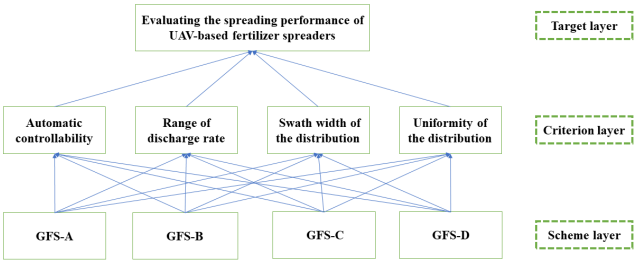

FIGURE 5. The hierarchy model of the critical indices.

The set of all relative comparisons in the hierarchy model was reported in a square matrix, in which the elements were compared with each other. As shown in Table 4, the comparisons, on a scale ranging from 1 to 9, corresponded to the level of dominance or of contribution to the target. The values in the diagonal of the matrix were always 1 (when compared with itself, each alternative had equal importance), and the values in the lower triangle of the matrices are the reciprocal values of the upper triangle. Therefore, pairwise comparisons were required for only half of the matrix, excluding the diagonal. The pairwise comparison matrices for the criterion layer and the scheme layer were constructed in a similar way.

TABLE 4. Rules of pairwise comparison scale.

Rating	Description
1	Both alternatives have equal importance.
3	One of the alternatives is slightly more important than the other.
5	One of the alternatives is more important than the other.
7	One of the alternatives is much more important than the other.
9	One of the alternatives is strictly superior to the other.
2, 4, 6, 8	The ratio of the two alternatives is between the adjacent ratings.
1, 1/2, ……, 1/9	The importance of both alternatives is the inverse of the latter to the former.

A consistency check was performed by calculating the consistency index (CI) and the consistency ratio (CR). When CR<0.1, the consistency of the comparison matrix was considered acceptable; otherwise, the comparison matrix should be appropriately modified. Equations (4) and (5) were used to calculate the value of the CR.

$$CI = \frac{M-n}{n-1} \tag{4}$$

$$\mathrm{CR} = \frac{CI}{RI} \tag{5}$$

where M is the maximum eigenvalue of the target matrix; n is the target matrix order; and RI is the random consistency index acquired by consulting a table.

An AHP web-based calculation and Excel software were used to calculate the normalized eigenvectors (namely, priority weights) of the pairwise comparison matrices of the criterion layer and the scheme layer. The priority weights had two types: local priority weights and global priority weights. The local priority weights represented the relative weights of the schemes within a group of indices with respect to their evaluation indices. The local priority weights were derived from each set of pairwise comparisons in each level of the scheme matrix. The global priority weights were obtained by multiplying the local priorities of the schemes by the priority weights of the indices in the criterion layer. A high priority weight value indicated the priority of the numerical model that it represented. In this process, the importance of each local scheme was balanced by the importance of the index to which it belonged. Then, the acceptability of the result was verified by a hierarchical total sort consistency check. The following equations can be used to calculate the priority weights:

$$W_0 = \{W_A, W_B, W_C, W_D\} \tag{6}$$

$$\mathrm{W} = W_0 \times Q^T \tag{7}$$

where W_0 is the group of the normalized eigenvectors of the scheme matrices; $W_{A,B,C,D}$ are the normalized eigenvectors of each scheme, which are the local priority weights; Q is the normalized eigenvector of the criterion matrix, which is the priority weight of each index; and Q^T is the transposed version of matrix Q.

III. RESULTS AND DISCUSSIONS

A. CONTROLLABLE DISCHARGE PROPERTIES

Of the four UAV-based GFSs, GFS-A had the maximum controllable discharge range at 4.95-27.16 kg/min, while GFS-B had the minimum at 0-3 kg/min, and GFS-C and GFS-D had 2.21-19.36 kg/min and 1.16-10.27 kg/min, respectively. In addition, different discharge rates could be acquired for GFS-B, C and D by remote control, while that of GFS-A was adjusted by manually replacing the annulus with different diameters. The relationships between the variable opening gate and the actual discharge rate are shown in Fig. 6. The three regression curves for GFS-B, C and D, which have stepless discharge adjustment, were plotted, and the regression equations are given in equations (8)-(10).

$$y_1 = -0.0004{x_1}^2 + 0.0665x_1 + 0.5184 \times (\mathrm{R}^2 = 0.8812) \tag{8}$$

$$y_2 = 0.0089{x_2}^2 - 0.5013x_2 + 7.0885 \times (\mathrm{R}^2 = 0.9947) \tag{9}$$

$$y_3 = 0.1677x_3 + 0.3788 \quad (\mathrm{R}^2 = 0.9991) \tag{10}$$

where $\mathrm{y}_{1,2,3,}$ = the discharge rate of GFS-B, C or D, kg/min; x_1 = the straight board opening percentage, %; x_2 = the butterfly damper angle, °; and x_3 = the rotational speed, r/min.

For the discharge rate, the range in Fig. 6(b) is suitable for the small quantity requirements of precision field application,

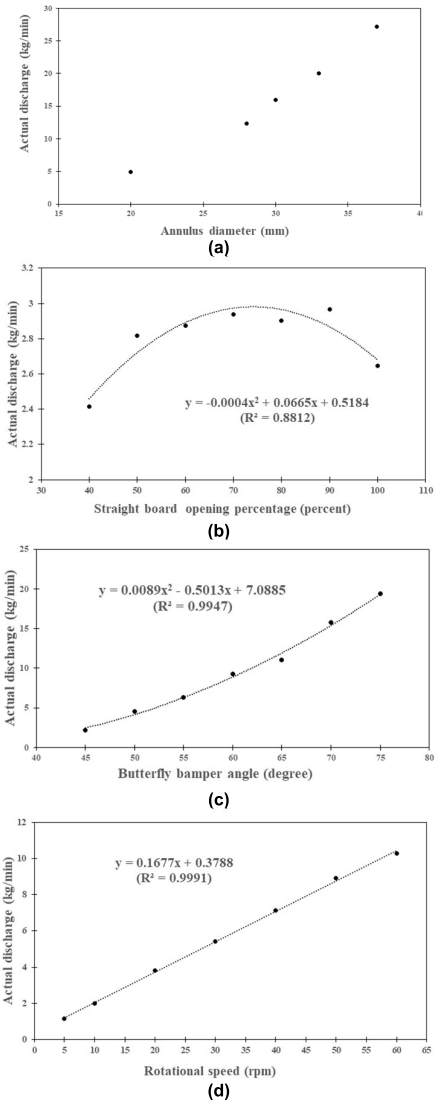

FIGURE 6. Discharge properties of four metering devices. (a) GFS-A-annulus (b) GFS-B-straight board (c) GFS-C-butterfly valve (d) GFS-D-fluted roller.

and the results in Fig. 6(a), (c) and (d), corresponding to GFS-A, C and D, respectively, indicate that they can be used in large-scale field applications with large discharge quantity requirements. Fig.6(d) shows the simplest relationship between discharge rate and rotational speed, making it easy to realize variable-rate adjusting fertilizer discharge rate.

B. DISTRIBUTION PATTERN OF UAV-BASED GFS

1) DEPOSITION IN THE COLLECTION AREA

The collection results are shown in Fig. 7. At the end of each collection line, there was almost no urea deposition, and this level of deposition was considered as zero. The deposition in all three collection lines for each UAV-based GFS revealed the same change trend on the whole, proving the validity of this method for presenting the distribution pattern. As shown in Fig. 7(a), the deposition at most collection points on the

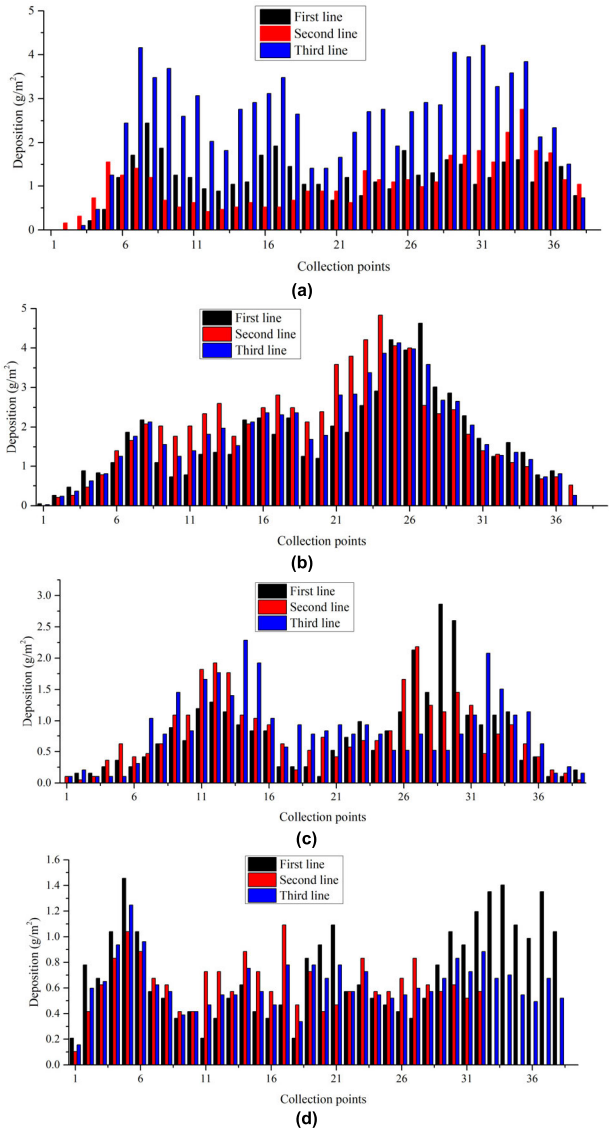

FIGURE 7. Deposition distributions of the four UAV-based GFSs. (a) GFS-A-centrifugal disc spreader. (b) GFS-B-centrifugal disc spreader. (c) GFS-C-pneumatic double-duct spreader. (d) GFS-D-pneumatic multi-duct spreader.

third line is obviously higher than that on the other two lines. This may have been due to the wind field generated from the double propellers on each arm of GFS-A, which was stronger than the other UAV-based GFSs in the test when working at the same height. In such a wind field, when the UAV-based GFS flies above the collection carpet, some urea particles that fell on the two previous collection lines were blown to the last line and accumulated. As shown in Fig. 7(b), the deposition on the left side of the flight centerline was lower than that on the other side, showing an asymmetrical deposition distribution. Meanwhile, there are two obvious peaks of deposition at symmetrical collection points across the flight centerline in Fig. 7(c). The deposition pattern shown in Fig. 7(d) fluctuates slightly across all the collection points, except that at the right end of the second collection line, there is no deposition, and at the left end of all collection lines, there is slightly higher deposition.

The total deposition of the four UAV-based GFSs for all three collection lines was calculated. As shown in Fig. 8, except for the specific distribution of GFS-A, the maximal deviation among the three lines is less than 12 g/m^2 for GFS-B, C and D, presenting good uniformity in the forward direction. The mean line shows that the overall deposition of GFS-B is higher than the others, resulting from its slower travel speed used in the test to obtain an obvious deposition pattern in the collection lines.

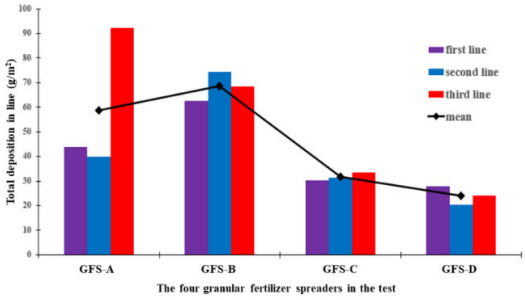

FIGURE 8. Total deposition in all collection areas for four UAV-based GFSs.

2) ANALYSIS OF DISTRIBUTION PATTERN

Variability of deposition distribution across the swath for different spreaders can be significantly influenced by movement properties of the urea being spread out. Fig. 9 illustrates the distribution patterns of the four UAV-based GFSs in the test. The distribution pattern of GFS-A is a trapezoid. The horizontal leg of the trapezoid covers 75 % of the swath width, and the deposition frequently covers in a larger range of 1-2.5 g/m^2, indicating the substantial changes in deposition from collection points 7 to 34. The two shoulders of trapezoid show a monotonic change trend, with one increasing and the other decreasing. In addition, the deposition at some collection points on the right side is more than that at collection points near the centerline. This difference in deposition weakens the distribution uniformity when considering the two sides of a single swath. This is difficult to optimize by just changing the flight mode, and improvement of the structure and control method may be useful.

The distribution pattern of GFS-B is a wide triangle with obviously asymmetrical sides. It is obvious that the left side of the triangle, which shows a gentle change trend, occupies more than half of the swath width, and the right side shows a sharp decrease in deposition. This phenomenon, called skewness, has a pronounced effect on the deposition distribution across the swath width. Therefore, for GFS-B, it is important to control the position of the particle flow on the disc board, which is the main factor generating a deposition distribution that is perpendicular to the flight centerline, as the disc rotates in a single direction.

The distribution pattern of GFS-C is a typical M-shape with two peaks. The deposition at the peak points is three

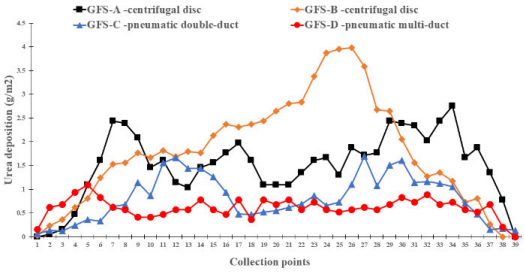

FIGURE 9. Distribution patterns of the four UAV-based GFSs.

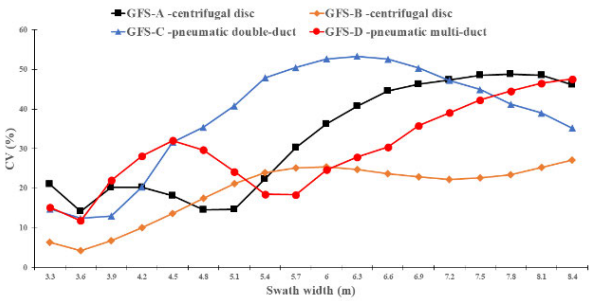

FIGURE 10. The CV-swath width curves of the distribution patterns of four UAV-based GFSs.

times as high as the deposition at other points. These two peaks correspond to the two independent tube branches of the double-duct structure in GFS-C. Two concentrated distribution areas that correspond to the two main outlets are generated, with similar distribution pattern of a high deposition in the center and a decrease at both ends. Once these two distribution areas overlap improperly, the M-shaped pattern is generated. Changing the angle of the double-duct branches to adjust this overlap is suggested for field application.

The distribution pattern of GFS-D is similar to the previously described wide trapezoidal shape, but it has narrow shoulders at both ends, where the horizontal leg of the trapezoid covers more than 90 % of the total swath width. Furthermore, except for the high deposition at the left end, which was probably caused by fight instability, the deposition deviation of the horizontal leg of the trapezoid is approximately 0.6 g/m^2, indicating a slight change in the deposition distribution.

C. SWATH WIDTH AND DISTRIBUTION UNIFORMITY

In general, a coefficient of variation lower than 15% will result in an acceptable uniform application of the applied mean dosage [27]. However, even with an acceptable distribution uniformity, a large spread width is also necessary to improve work efficiency in field applications. Studies have illustrated that a CV of 20-30% was a reasonable uniformity for granular fertilizer spreaders under some farm conditions [28], [29]. Additionally, previous studies have suggested that uniformity can be as low as 5-10% and as high as 30% under actual field terrain conditions[30]. Grift showed that the CV value fluctuated below the acceptable uniformity standard line (generally CV = 15%) at a smaller swath width, yet the CV value increased quickly as the simulated swath width increased when testing the larger swath width for a high-quality distribution pattern [31]. Particularly, for wide trapezoidal shapes with narrow shoulders, more incremental swath width simulations should be performed to reveal the integrated change tendency. Therefore, a conservative swath width (where CV = 20% is set as the standard) may be considered the optimal swath interval for UAV-based GFS under the same conditions as the test.

Fig. 10 shows the simulated relationship between the CV and the swath width of the distribution pattern. Except for that of GFS-C, which had an inferior distribution pattern, all the other curves changed in the same way along the given swath width on the whole, indicating the rationality and validity of this simulated relationship. For GFS-A, both CVs at the bottom of the curve are under 20%; generally, it is reasonable that a larger swath width (5.1 m) would be used as the effective flight interval. Similarly, the other trapezoidal shape, the distribution pattern of GFS-D, shows an acceptable fluctuation with a hump before a monotonical increase; in this case, a swath width of 5.7 m (CV = 18.36%) is the recommended value. For GFS-B and GFS-C, there is only one minimum in each of the CV-swath width curves where the CV is under 20%. In particular, for GFS-B, almost half of the curve is under the uniformity standard line (CV $\leq$ 20%), and the second reflection point is slightly above the standard line, which was caused by the asymmetrical triangle shape of the distribution pattern. In this case, a swath width related to the minimum CV (4.28%) may not be the optimal choice when taking the environmental conditions into account. Overall, flight intervals of 4.8 m (CV = 17.55%) and 3.9 m (CV = 13.02%) may be preferred for the use of GFS-B and GFS-C in the field application of urea.

In short, GFS-D showed better spreading performance in terms of swath width and distribution uniformity than the others in this study. Although the actual deposition distribution of UAV-based GFSs is observably affected by complex factors [32], the uniformity of the single-pass distribution pattern may have a great influence on the overall uniformity of the overlapping deposition area. The swath width and distribution uniformity of the four kinds of distribution pattern also demonstrate the reasonability of this method and provide a reference for the further improvement of distribution uniformity in field applications.

D. RESULTS OF THE COMPREHENSIVE EVALUATION

1) PAIRWISE COMPARISONS AND CONSISTENCY CHECK

The priority of each factor was captured by determining the importance of each factor with respect to the others in the same category using a pairwise comparison scale as described in Table 4. The indices were also compared with each other. The data were entered into pairwise comparison matrices as scores on the pairwise comparison scale. A sample pairwise comparison matrix for the four evaluation indices is depicted

in Table 5. The values in the cells of the matrix representing the results of the weighting (each cell shows the relationship between the alternative in the row and the alternative in the column) were collected by questionnaires within the agricultural machine and fertilization industry. The results of the consistency check (CR $<$ 0.1) showed that the consistency of the comparison matrix was considered acceptable.

TABLE 5. Pairwise comparison matrix of criterion layer.

Index	Automatic controllability	Range of discharge rate	Swath width of the distribution	Uniformity of the distribution
Automatic controllability	1.0000	4.0000	1.5000	3.0000
Range of discharge rate	0.2500	1.0000	0.2500	0.5000
Swath width of the distribution	0.6667	4.0000	1.0000	2.0000
Uniformity of the distribution	0.3333	2.0000	0.5000	1.0000

In this matrix, the element in row 1, column 4 is 3, which indicates that automatic controllability was slightly more important than uniformity of distribution. The element in row 4, column 1 is 0.3333, which indicates that uniformity of distribution was judged to be slightly more important than automatic controllability.

The pairwise comparison matrix of scheme layer was constructed similarly and is shown in Table 6. The results of the consistency check (CR $<$ 0.1 for each of the pairwise comparison matrices) show that all of the pairwise comparison matrices were acceptable for use in the analysis of the priority of these schemes for each evaluation index.

2) COMPUTION OF THE PRIORITY WEIGHTS

The priority order of the evaluation indices was determined according to the importance of these four evaluation indices in the comprehensive evaluation, and the normalized eigenvector (11) showed their priority weights, namely, the importance order of the four evaluation indices were automatic controllability, range of discharge rate, swath width and uniformity of the distribution. Automatic controllability was the most important index among them due to the necessity of remote control of UAV-based GFSs.

The local priority weights of each scheme are shown in the normalized eigenvector (12), meaning that the matrix W_0 consisted of the priority order of all schemes in each evaluation index taking performance into consideration. For example, the first column of matrix W_0 shows that in regard to automatic controllability, the maximum value in row 4 indicates that GFS-D performed better than the rest of the schemes, and the minimum value in row 1 has the opposite meaning; this value is consistent with the reality that GFS-A cannot be controlled automatically. In the same way, the second column of matrix W_0 indicates the priority order of these schemes in the range of discharge rates, and GFS-C performed better than the others. The rest of matrix W_0 provides the same information for the other two evaluation indices and highlights the good performance of GFS-D in terms of swath width and uniformity.

TABLE 6. Pairwise comparison matrix for scheme layer.

	GFS-A	GFS-B	GFS-C	GFS-D
	Automatic controllability			
GFS-A	1.0000	0.2500	0.5000	0.2000
GFS-B	4.0000	1.0000	2.0000	0.6667
GFS-C	2.0000	0.5000	1.0000	0.3333
GFS-D	5.0000	1.5000	3.0000	1.0000
	M	CI	RI	CR
	4.0042	0.0014	0.9	0.0016
	Range of discharge rate			
GFS-A	1.0000	2.0000	0.3333	0.4000
GFS-B	0.5000	1.0000	0.2000	0.2500
GFS-C	3.0000	5.0000	1.0000	1.2000
GFS-D	2.5000	4.0000	0.8333	1.0000
	M	CI	RI	CR
	4.0053	0.0018	0.9	0.0020
	Swath width of the distribution			
GFS-A	1.0000	1.5000	3.0000	0.7500
GFS-B	0.6667	1.0000	2.0000	0.5000
GFS-C	0.3333	0.5000	1.0000	0.3333
GFS-D	1.3333	2.0000	3.0000	1.0000
	M	CI	RI	CR
	4.0103	0.0034	0.9	0.0038
	Uniformity of the distribution			
GFS-A	1.0000	0.5000	1.0000	0.5000
GFS-B	2.0000	1.0000	0.5000	1.0000
GFS-C	1.0000	2.0000	1.0000	0.5000
GFS-D	2.0000	1.0000	2.0000	1.0000
	M	CI	RI	CR
	4.2492	0.0831	0.9	0.0923

$$Q^T = \left\{0.9924, 9.0152\text{E}^{-12}, 0.0077, 1.1671\text{E}^{-7}\right\} \tag{11}$$

$$W_0 = \begin{Bmatrix} 1.5194\text{E}^{-12}, 4.6055\text{E}^{-8}, 0.0307, 1.5140\text{E}^{-5} \\ 0.0031, 3.5577\text{E}^{-12}, 4.6742\text{E}^{-5}, 0.0039 \\ 4.8019\text{E}^{-8}, 0.9561, 2.2532\text{E}^{-9}, 0.0039 \\ 0.9969, 0.0439, 0.9693, 0.9922 \end{Bmatrix} \tag{12}$$

$$W^T = \left\{0.0002, 0.0031, 4.8130\text{E}^{-8}, 0.9966\right\} \tag{13}$$

The normalized eigenvector (13) was obtained to represent the global priority of the hierarchical total sort by comprehensively considering the priorities of the criterion layer and scheme layer. The result of the consistency check for the hierarchical total sort was a CR of 0.0016 (CR $<$ 0.1), indicating the validity and acceptability of the normalized eigenvector W^T for explaining the combined priority weights of the factors. This result shows that the comprehensive performance of GFS-D is better than that of the others in terms of automatic fertilization, which is beneficial for variable-rate control of fertilizer application rate.

IV. CONCLUSION

In this study, four UAV-based GFSs with different discharge structures and control mechanisms were compared in terms of their controllable range of discharge rate and variable-rate control mode, deposition and distribution pattern, swath width and distribution uniformity to evaluate their comprehensive performance. The features and shortcomings of these four UAV-based GFSs were analyzed according to these evaluation indices. Among them, the metering device of GFS-A was suitable for uniform discharge rate; the controllable discharge range of GFS-B could be sufficient for the application of small range of discharge rate; and the granular deposition distribution pattern of GFS-C was M-shaped, resulting in obvious fluctuation along the transverse direction, which was related to the distribution uniformity. Proper adjustment in the angle of outlets is needed to improve the uniform distribution as well as the effective swath width. The simulated swath width and distribution uniformity indicated better spreading performance by GFS-D, which had a larger effective swath width with an acceptable uniformity. In fact, the score for GFS-D based on the combined priorities of the evaluation indices calculated using AHP method was higher than those for the three other UAV-based GFSs, demonstrating its superior performance as a UAV-based GFS prototype for precision variable-rate fertilization at a large range of application rate. Further work is planned to design an automatic variable-rate control system for precise site-specific fertilizer management.

ACKNOWLEDGMENT

The authors gratefully acknowledge those UAV companies for applying UAV-based GFS and technology suggestions. Also, they wish to thank their fellows and participator from cooperative department for their assistance during the test. The authors also wish to thank sincerely the editors and anonymous reviewers for their critical comments and suggestions to improve the manuscript..

REFERENCES

[1] A. A. Alameen, K. A. Al-Gaadi, and E. Tola, "Development and performance evaluation of a control system for variable rate granular fertilizer application," *Comput. Electron. Agricult.*, vol. 160, pp. 31–39, May 2019, doi: 10.1016/j.compag.2019.03.011.

[2] S. C. Hassler and F. Baysal-Gurel, "Unmanned aircraft system (UAS) technology and applications in agriculture," *Agronomy*, vol. 9, no. 10, p. 618, Oct. 2019, doi: 10.3390/agronomy9100618.

[3] H. Zhu, H. Li, C. Zhang, J. Li, and H. Zhang, "Performance characterization of the UAV chemical application based on CFD simulation," *Agronomy*, vol. 9, no. 6, p. 308, Jun. 2019, doi: 10.3390/agronomy9060308.

[4] C. Song, "Design and test of centrifugal disc type sowing device for unmanned helicopter," *Int. J. Agricult. Biol. Eng.*, vol. 11, no. 2, pp. 55–61, 2018, doi: 10.25165/j.ijabe.20181102.3757.

[5] Y. A. Pederi and H. S. Cheporniuk, "Unmanned aerial vehicles and new technological methods of monitoring and crop protection in precision agriculture," in *Proc. IEEE Int. Conf. Actual Problems Unmanned Aerial Vehicles Develop. (APUAVD)*, Oct. 2015, pp. 298–301.

[6] D. D. K. Sreekantha, "Applications of unmanned ariel vehicles (UAV) in agriculture : A study," *Int. J. for Res. Appl. Sci. Eng. Technol.*, vol. 6, no. 5, pp. 1162–1166, May 2018, doi: 10.22214/ijraset.2018.5188.

[7] Y. Lan, C. Shengde, and B. K. Fritz, "Current status and future trends of precision agricultural aviation technologies," *Int. J. Agricult. Biol. Eng.*, vol. 10, no. 3, pp. 1–17, May 2017.

[8] M. A. Latif, "An agricultural perspective on flying sensors: State of the art, challenges, and future directions," *IEEE Geosci. Remote Sens. Mag.*, vol. 6, no. 4, pp. 10–22, Jul. 2018, doi: 10.1109/MGRS.2018.2865815.

[9] D. Yamunathangam, J. Shanmathi, R. Caviya and G. Saranya, "Payload manipulation for seed sowing unmanned aerial vehicle through interface with pixhawk flight controller," in *Proc. 4th Int. Conf. Inventive Syst. Control (ICISC)*, Jan. 2020, pp. 931–934.

[10] F. Zakharin and S. Ponomarenko, "Unmanned aerial vehicle integrated navigation complex with adaptive tuning," in *Proc. IEEE 4th Int. Conf. Actual Problems Unmanned Aerial Vehicles Develop. (APUAVD)*, Oct. 2017, pp. 23–26.

[11] G. Gyarmati and T. Mizik, "The present and future of the precision agriculture," in *Proc. IEEE 15th Int. Conf. Syst. Syst. Eng. (SoSE)*, Jun. 2020, pp. 593–596.

[12] J. Li, "Design and test of operation parameters for rice air broadcasting by unmanned aerial vehicle," *Int. J. Agricult. Biol. Eng.*, vol. 9, no. 5, pp. 24–32, 2016.

[13] Z. Wu, M. Li, X. Lei, Z. Wu, C. Jiang, L. Zhou, R. Ma, and Y. Chen, "Simulation and parameter optimisation of a centrifugal rice seeding spreader for a UAV," *Biosyst. Eng.*, vol. 192, pp. 275–293, Apr. 2020, doi: 10.1016/j.biosystemseng.2020.02.004.

[14] F. Cointault, P. Sarrazin, and M. Paindavoine, "Measurement of the motion of fertilizer particles leaving a centrifugal spreader using a fast imaging system," *Precis. Agricult.*, vol. 4, pp. 279–295, Sep. 2003.

[15] J. P. Fulton, S. A. Shearer, T. S. Stombaugh, and S. F. Higgins, "Pattern assessment of a spinner disc variable-rate fertilizer applicator," in *Proc. ASAE Annu. Int. Meeting*. Sacramento, CA, USA: Sacramento Convention Center, Aug. 2001, Paper 01-1116.

[16] C. Song, Z. Zhou, R. Jiang, X. Luo, X. He, and R. Ming, "Design and parameter optimization of pneumatic rice sowing device for unmanned aerial vehicle," *Trans. Chin. Soc. Agricult. Eng.*, vol. 34, no. 6, pp. 80–88, 2018.

[17] O. Miserque, E. Pirard, Y. Schenkel, O. Mostade, and B. Huyghebaert, "Spreading segregation of blended fertilizers: Influence of the particles properties," *Appl. Eng. Agricult.*, vol. 24, no. 2, pp. 137–144, 2008.

[18] J. P. Fulton, S. A. Shearer, S. F. Higgins, and T. P. McDonald, "A method to generate and use as-applied surfaces to evaluate variable-rate fertilizer applications," *Precis. Agricult.*, vol. 14, no. 2, pp. 184–200, Apr. 2013, doi: 10.1007/s11119-012-9286-1.

[19] T. E. Grift, "Spread pattern analysis tool (SPAT): I. Development and theoretical examples," *Trans. ASAE*, vol. 43, no. 6, pp. 1341–1350, 2000, doi: 10.13031/2013.3031.

[20] Y. Wang and W. Zhang, "Four-rotor UAV virtual simulation system for agricultural sowing," in *Proc. IEEE 4th Inf. Technol. Mechatronics Eng. Conf. (ITOEC)*, Dec. 2018, pp. 1097–1101.

[21] S. Zeng, Y. Tan, Y. Wang, X. Luo, L. Yao, D. Huang, Z. Mo," *Int. J. Agricult. Biol. Eng.*, vol. 13, no. 2, pp. 101–110, 2020, doi: 10.25165/j.ijabe.20201302.4999.

[22] *Calibration and Distribution Pattern Testing of Agricultural Aerial Application Equipment*, ASAE Standard S386.2., 2013.

[23] S. May and H. Kocabiyik, "Design and development of an electronic drive and control system for micro-granular fertilizer metering unit," *Comput. Electron. Agricult.*, vol. 162, pp. 921–930, Jul. 2019, doi: 10.1016/j.compag.2019.05.048.

[24] *Procedure for Measuring Distribution Uniformity and Calibrating Granular Broadcast Spreaders*, ASAE S341.3 FEB04, 2006.

[25] W. Zhang, "Analytic hierarchy process (AHP): MATLAB computation software," *Netw. Biol.*, vol. 9, no. 1, pp. 10–17, 2019.

[26] V. Pereira and H. G. Costa, "Nonlinear programming applied to the reduction of inconsistency in the AHP method," *Ann. Oper. Res.*, vol. 229, no. 1, pp. 635–655, Jun. 2015, doi: 10.1007/s10479-014-1750-z.

[27] D. R. Gardisser, "Computer simulation of dry material distribution patterns from agricultural aircraft," Ph.D. dissertation, Univ. Arkansas, Fayetteville, AR, USA, 1992.

[28] D. B. SmithD Oakley and E. Williams, "Broadcast spray deposits from fan nozzles," *Appl. Eng. Agricult.*, vol. 16, no. 2, p. 109, 2000.

[29] C. R. Crozier and G. T. Roberson, "Granular fertilizer spreader swath uniformity achieved at varying target application rates," *Crop Manage.*, vol. 13, no. 1, pp. 1–6, 2014, doi: 10.2134/CM-2013-0103-RS.

[30] Y. D. F. DialloS To and D. B. Smith, "Buggy flow rates and truck/buggy pattern comparisons of granular spreaders," *Appl. Eng. Agricult.*, vol. 20, no. 3, pp. 297–303, 2004.

[31] T. E. Grift, "Spread pattern analysis tool (SPAT): II. Examples of aircraft pattern analysis," *Trans. ASAE*, vol. 43, no. 6, pp. 1351–1362, 2000, doi: 10.13031/2013.3032.

[32] V. D. Young, R. G. Winterfeld, C. E. Deonier, and C. W. Getzendaner, "Factors influencing the deposit position of granular materials applied by aircraft at low-flight levels with fixed-wing aircraft," *Trans. ASAE*, vol. 9, no. 5, pp. 665–668, 1966, doi: 10.13031/2013.40066.

CANCAN SONG received the M.E. degree in agricultural electrification and automation from South China Agricultural University, Guangzhou, China, in 2018, where she is currently pursuing the Ph.D. degree with the College of Engineering.

Her current research interests include variable-rate technology, intelligent control systems, and the granular distributor of UAV.

YING ZANG received the Ph.D. degree from China Agricultural University, Beijing, China, in 2003. Since 2007, she has been a Professor of the College of Engineering, South China Agriculture University, Guangzhou, China.

From 2013 to 2014, she was a Visitor Scholar of Texas A&M University, USA. She is a Senior Member of the Chinese Society of Agricultural Engineering, also a member of the American Society of Agricultural and Biological Engineers (ASABE) and the National Agricultural Aviation Association (NAAA), also the Deputy Director of the Agricultural Aviation Branch, Chinese Society for Agricultural Machinery (CSAM), and also the Deputy Secretary-General of Technology Innovation Strategic Alliance for Agricultural Aviation. Her current research interests include rice precise seeding machine and plant protection of agricultural aviation, soil sensor technology, and rice paddy information collection technology.

ZHIYAN ZHOU received the Ph.D. degree in agricultural electrification and automation from South China Agricultural University, Guangzhou, China, in 2011.

From 2012 to 2014, he held a postdoctoral position and a Visitor Scholar of the U.S. Department of Agriculture, Agricultural Research Service, Aerial Application Technology Research Unit (USDA-ARS-AATRU), USA. Since 2006, he has been with the College of Engineering, South China Agricultural University, Guangzhou, China, where he is currently a Professor, also the Deputy Director of the National Center for International Collaboration Research on Precision Agricultural Aviation Pesticides Spraying Technology (NPAAC), also a member of the professional working group of the civil unmanned aerial vehicle inspection method, also the Secretary-General of the Technology Innovation Strategic Alliance for Agricultural Aviation (TISAAA), and also a member of the American Society of Agricultural and Biological Engineers (ASABE) and the National Agricultural Aviation Association (NAAA). He has already declared 46 Chinese patents (28 authorized) and one PCT patents. His current research interests include agricultural aviation, and Internet of Things in agriculture and intelligent detection and control.

XIWEN LUO received the B.E. degree in radio technology from the Huazhong University of Science and Technology, Hubei, China, in 1970, and the M.E. degree in agricultural electrification and automation from South China Agricultural University, Guangzhou, China, in 1982.

From 1992 to 1996, he was the Dean of the Department of Agricultural Engineering, College of Engineering and Technology, South China Agricultural University, and also the Vice President of South China Agricultural University, from 1996 to 2006. He is currently an Academician of the Chinese Academy of Engineering, and also a Professor of South China Agricultural University, where he is also the Director of the Key Laboratory of Key Technology on Agricultural Machine and Equipment, Ministry of Education. His current research interests include agricultural aviation and intelligent detection and control.

LINGLI ZHAO received the B.E. degree in mechanical manufacture and automation from the University of South China, Hengyang, China, in 2018. She is currently pursuing the M.D. degree with the College of Engineering, South China Agricultural University, Guangzhou, China.

Her current research interests include biological release delivery technology, precision delivery systems, and the biological release delivery device of UAV.

RUI MING received the B.E. degree in mechanical design manufacture and automation from Hubei Polytechnic University, Hubei, China, in 2016. He is currently pursuing the Ph.D. degree with the College of Engineering, South China Agricultural University, Guangzhou, China.

His current research interests include formation control, neural network control, and intelligent control systems.

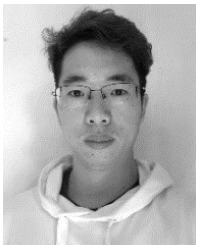

LE ZI received the B.E. degree in electrical engineering and automation from Southwest Jiaotong University, Sichuan, China, in 2017. He is currently pursuing the M.E. degree with the College of Engineering, South China Agriculture University, Guangzhou, China.

His current research interests include motor control, information transmission, and intelligent control systems.

YU ZANG received the Ph.D. degree in engineering from the Department of Agricultural Mechanization Engineering, South China Agricultural University, Guangzhou, in 2019.

From 2014 to 2017, he experimented with the application of cotton defoliant by UAV for four consecutive years in Xinjiang. From 2017 to 2019, he conducted a series of spray atomization experiment in the wind tunnel and the physicochemical properties of the spray adjuvant. He joined the International Laboratory of Agricultural Aviation Pesticide Spraying Technology, National Center for International Collaboration Research on Precision Agricultural Aviation Pesticide Spraying Technology in 2016. His current research interests include the screening of spray adjuvants for the UAV and the optimization of UAV operation parameters.